C$_{60}$-induced Devil's Staircase transformation on a Pb/Si(111) wetting layer

Lin-Lin Wang,[1] Duane D. Johnson,[1,2,3] and Michael C. Tringides[1,3]

[1]*Ames Laboratory, U.S. Department of Energy, Ames, Iowa 50011, USA*
[2]*Department of Materials Science and Engineering, Iowa State University, Ames, Iowa 50011, USA*
[3]*Department of Physics, Iowa State University, Ames, Iowa 50011, USA*

Density functional theory is used to study structural energetics of Pb vacancy cluster formation on C$_{60}$/Pb/Si(111) to explain the unusually fast and error-free transformations between the "Devil's Staircase" (DS) phases on the Pb/Si(111) wetting layer at low temperature ($\sim$110 K). The formation energies of vacancy clusters are calculated in C$_{60}$/Pb/Si(111) as Pb atoms are progressively ejected from the initial dense Pb wetting layer. Vacancy clusters larger than five Pb atoms are found to be stable with seven being the most stable, while vacancy clusters smaller than five are highly unstable, which agrees well with the observed ejection rate of $\sim$5 Pb atoms per C$_{60}$. The high energy cost ($\sim$0.8 eV) for the small vacancy clusters to form indicates convincingly that the unusually fast transformation observed experimentally between the DS phases, upon C$_{60}$ adsorption at low temperature, cannot be the result of single-atom random walk diffusion but of correlated multi-atom processes.

I. INTRODUCTION

Pattern formation in heteroepitaxial overlayers via self-assembly at nano and mesoscale has attracted intensive research [1–6]. Among them the compressed two-dimensional (2D) wetting layer of Pb on Si(111) has generated great interest recently because a range of experiments at low temperature (T) have shown superfast diffusion [7–10] and explosive nucleation [11] during phase transformation in this system by fine tuning the Pb coverage (θ). A recent scanning tunneling microscopy (STM) experiment [12] showed that such exceptionally fast and anomalous mass transport can also be induced by the adsorption of C$_{60}$ on the Pb/Si(111) wetting layer at $T \sim$ 110 K with C$_{60}$ ejecting Pb atoms to transform the nearby region from an initial to a final Devil's staircase (DS) phase with slightly higher θ [13,14]. Although theoretical models with long-range elastic interaction included have studied some aspects of the pattern formation [15] and collective diffusion [16] in this compressed 2D system, essential information about the atomic level energy landscape in terms of single vs multi-atom processes is still lacking.

The adsorption of C$_{60}$ on the Pb/Si(111) wetting layer [12] offers an opportunity to unveil such energy landscape. C$_{60}$ can eject a different number of substrate atoms and generate vacancies of different sizes, i.e., a single vacancy on Al [17,18], Pt [19,20], Ag [21,22], and Au [23–25] (111) surfaces while a seven-atom nanopit on Cu(111) [26,27]. Here, using density functional theory (DFT) [28,29] to calculate the formation energies of Pb vacancy clusters by incrementally removing Pb atoms from the wetting layer in C$_{60}$/Pb/Si(111), we map out the thermodynamic stability of the vacancy clusters as a function of cluster size. The calculated energy landscape clarifies further the puzzling experimental observations.

Some DS phases [13] of the highly compressed wetting layer of Pb/Si(111) are schematically shown in Fig. 1 (with the atomic structures related to the C$_{60}$/Pb/Si(111) experiment [12]). On the left, the surface unit cells of the ($\sqrt{3} \times \sqrt{7}$) and ($\sqrt{3} \times \sqrt{3}$) phases are shown [defined in terms of the underlying Si(111) layer]. They contain six (four) Pb atoms

per five (three) Si atoms in the ($\sqrt{3} \times \sqrt{7}$) [($\sqrt{3} \times \sqrt{3}$)] unit cell; thus $\theta = 6/5(4/3)$ monolayer (ML) or 1.20 (1.33) ML. The DS phases are linear combinations generated from these two phases for $1.20 < \theta < 1.33$ ML, as θ is increased gradually. In STM and spot-profile-analysis low energy electron diffraction (SPA-LEED) experiments, 12 and 16 DS phases have been atomically resolved, respectively [13]. The observation of such a large number of discrete thermodynamically stable phases within such a narrow coverage range ($\sim$0.09 ML) is one of the best realizations of a DS in nature. For example, the DS(2,1) phase is formed by two units of ($\sqrt{3} \times \sqrt{7}$) and one unit of ($\sqrt{3} \times \sqrt{3}$) along the $\langle 1\bar{1}0 \rangle$ direction appearing as long rows along $\langle 11\bar{2} \rangle$ in STM images. It was also shown [30] that with heating (from 120 to 350 K depending on the coverage of the initial DS phase), the linear phases transform into phases of different symmetry, the so-called hexagonal incommensurate phase (HIC) and stripe incommensurate phase (SIC). A recent STM experiment [12] found that on the DS of Pb/Si(111), even at $T \sim$ 110 K, the adsorption of C$_{60}$ is capable of ejecting on average five Pb atoms (as shown schematically on the right in Fig. 1). The ejected Pb atoms increase locally the Pb coverage and induce ideal structural transformation to the DS phase next in the hierarchy, despite the low T. Because these transformations are extremely fast (with completion times smaller than the STM acquisition speed of several tens of seconds), it was inferred that they must be the outcome of correlated multi-atom processes.

DFT calculations have provided insights to explain the experimental observations on C$_{60}$/metal interfaces [18,20–22,25–27,31–39]. Here we focus on the energetics of the Pb vacancy cluster formation induced by a C$_{60}$ ML on Pb/Si(111). We search for the lowest-energy structures in the C$_{60}$/Pb/Si(111)-($\sqrt{7} \times \sqrt{7}$) surface unit cell as Pb atoms are gradually removed from the system. We construct the formation energy (E_f) diagram as a function of the size of the Pb vacancy cluster (N_V), i.e., the number of the Pb atoms being ejected. We show that it is thermodynamically favorable to create Pb vacancy clusters with the size $N_V \geqslant 5$ per C$_{60}$ and
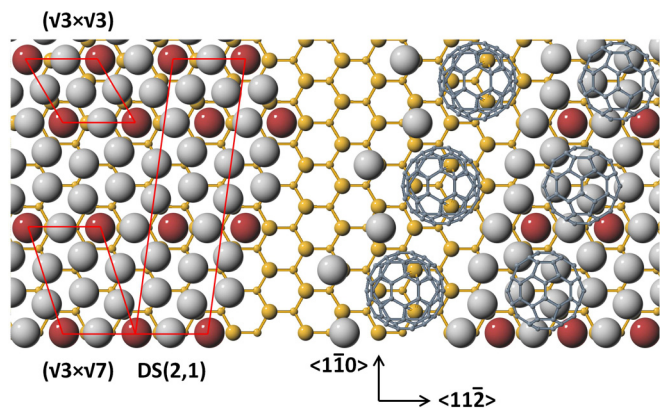
FIG. 1. (Color online) Devil's staircase (DS) phase transformation in a Pb/Si(111) wetting layer. Medium (small) brown spheres are Si atoms in the upper (lower) layer. Pb atoms appear as large gray and red spheres, with the latter sitting on the threefold hollow site of the underlying Si(111). The gray cages are C_{60} molecule. The surface unit cells of the DS generating $(\sqrt{3} \times \sqrt{7})$, $(\sqrt{3} \times \sqrt{3})$, and a DS(2,1) phase are highlighted in red on the left, with $\theta = 1.20$, 1.33, and 1.23 ML, respectively. DS phases seen in the experiments are formed in the range $1.20 < \theta < 1.33$ ML as a linear combination of $(\sqrt{3} \times \sqrt{7})$ and $(\sqrt{3} \times \sqrt{3})$. DS(2,1) is formed by two units of $(\sqrt{3} \times \sqrt{7})$ and one unit of $(\sqrt{3} \times \sqrt{3})$ along $\langle 1\bar{1}0 \rangle$ direction appearing as long rows along $\langle 11\bar{2} \rangle$ in STM images. On the right, C_{60} adsorption can induce such transformation from an initial to a final DS phase by ejecting Pb atoms which are incorporated extremely fast in completing the pattern of the new phase at low T.

$N_V = 7$ being the most stable, while clusters with $N_V < 5$ are highly unstable. This change of stability in N_V corresponds well to the experimental observations [12] of the ejection of five Pb atoms on average per C_{60}. The much stronger C_{60}-Si (compared to C_{60}-Pb) interaction provides the driving force for the high Pb depletion that causes the DS phase transformation.

II. COMPUTATIONAL METHODS

The DFT calculations have been carried out using the local density approximation (LDA) [40,41] and DF1-optPBE [42,43] exchange-correlation functionals, a plane-wave basis set and projector augmented wave [44] method as implemented in the Vienna atomic simulation package (VASP) [45,46]. DFT-LDA calculations have been shown to describe well the C_{60}/metal interfaces, to explain successfully the puzzle in work function change on noble metal surfaces after C_{60} adsorption [32,33]; and to predict the energetics of the surface reconstructions induced by C_{60} [20,21]; and even the different orientations of C_{60} at the single vacancy on Ag(111) and Au(111) [25]. To estimate the van der Waals (vdW) interaction in the system [38,47], DF1-optPBE has been used to check key results. We use a 400 eV kinetic energy cutoff, 12 Å vacuum layer, and $(6 \times 6 \times 1)$ k-point mesh with a Gaussian smearing of 0.05 eV. Total energies are converged to 1 meV/atom with respect to the size of vacuum and k-point mesh, and the magnitudes of the force on each atom were reduced below 0.02 eV/Å. The E_f of C_{60}/Pb/Si(111) are

calculated as a function of θ,

$$E_f(\theta) = \frac{1}{N_{\text{Si}}^{\text{surf}}} \left[E_{C_{60}/\text{Pb}/\text{Si}(111)} - E_{C_{60}} - N_{\text{Pb}} E_{\text{Pb}}^{\text{bulk}} - E_{\text{Si}(111)} \right],$$

(1)

where the coverage is defined as $\theta \equiv N_{\text{Pb}}/N_{\text{Si}}^{\text{surf}}$, with N_{Pb} and $N_{\text{Si}}^{\text{surf}}$ being the number of Pb and top-layer Si atoms in the surface unit cell. $E_{C_{60}/\text{Pb}/\text{Si}(111)}$, $E_{C_{60}}$, and $E_{\text{Si}(111)}$ are, respectively, the total energies of the structure, of free-standing C_{60} ML, and of the Si(111) substrate in the surface unit cell. For Pb, the fcc bulk energy $E_{\text{Pb}}^{\text{bulk}}$ is used as energy reference. E_f can also be regarded as a function of N_{Pb} (or N_V) per surface unit cell. Similar formula can also be used for the adsorption energy for the case of the wetting layer itself at different θ without C_{60} and the case of C_{60} on Si(111) without Pb. The low-energy structures at the given θ are explored by varying the orientation of C_{60} followed by thermal annealing in *ab initio* molecular dynamics (MD) until no lower-energy structures are found [48]. The Si(111) surface is modeled by a slab of six atomic layers with one side passivated with H.

For the study of the C_{60}-induced Pb ejection on Pb/Si(111), the $(\sqrt{3} \times \sqrt{7})$ surface unit cell at $\theta = 1.20$ ML cannot accommodate well a quasihexagonal array of C_{60} with a ~10 Å nearest-neighbor distance between fullerenes. Based on the calculated bulk lattice constant of 5.40 Å for Si and 4.88 Å for Pb, the area of the two (111) surface unit cells of 12.8 and 10.6 Å^2 have the ratio ~9/7. So we construct a $(\sqrt{7} \times \sqrt{7})$ hexagonal surface unit cell for Pb/Si(111) with $\theta = 9/7$ (or 1.29 ML). Figure 2(a) shows the structure and surface unit cell of the $(\sqrt{7} \times \sqrt{7})$ phase. To compare the stability of the $(\sqrt{7} \times \sqrt{7})$ phase to the other known phases for Pb/Si(111), we plot E_f as a function of θ in Fig. 2(b). The results agree well with previous DFT studies [49] on the known sub-ML phases. We find that the new $(\sqrt{7} \times \sqrt{7})$ structure is quite stable with
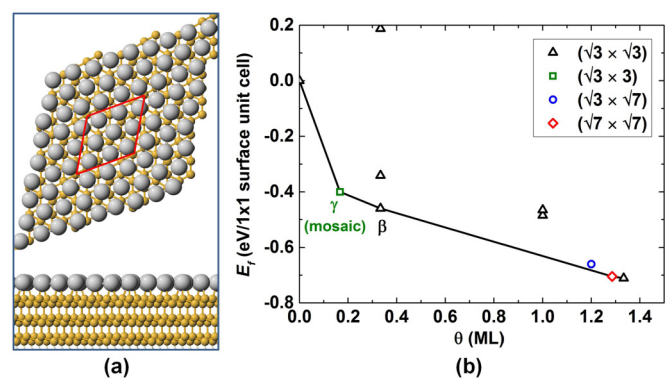

FIG. 2. (Color online) (a) Top and side view of the Pb wetting layer structure on Si(111) at 1.29 ML (nine Pb per seven Si atoms) with the $(\sqrt{7} \times \sqrt{7})$ surface unit cell highlighted in red. Large gray (small brown) spheres show Pb (Si) atoms. (b) Formation energy (E_f) per Si(111)-(1×1) surface unit cell for Pb/Si(111) at different coverage θ. Mosaic phase corresponds to Pb occupying the atop site of Si at $\theta = 1/6$ ML (see Figs. 2 and 3 in Ref. [49]). DS phases seen in the experiments formed in the range $1.20 < \theta < 1.33$ ML. The $(\sqrt{7} \times \sqrt{7})$ unit cell has similar energy as the $(\sqrt{3} \times \sqrt{3})$ phase and it can also accommodate the adsorption of C_{60}.

respect to the two generating phases of the DS structures, i.e., the ($\sqrt{3}\times\sqrt{7}$) at $\theta = 1.20$ ML and ($\sqrt{3}\times\sqrt{3}$) at $\theta = 1.33$ ML, and is on the ground-state (GS) hull. Within the ($\sqrt{7}\times\sqrt{7}$) unit cell, we can study the ejection of Pb atoms in C$_{60}$/Pb/Si(111) as N_V changes from 0 to 9.

III. RESULTS

Figure 3 plots E_f for the lowest-energy structures found by thermal annealing with *ab initio* MD in DFT for C$_{60}$/Pb/Si(111) as a function of Pb coverage, θ (or equivalently N_{Pb} or N_V), in the ($\sqrt{7}\times\sqrt{7}$) surface unit cell. The E_f is given both per Si(111)-(1×1) and per C$_{60}$. The selected atomic structures at $N_V = 0$, 3, and 7 are presented in Fig. 4 together with the electron density difference ($\Delta\rho = \rho_{C_{60}/Pb/Si(111)} - \rho_{C_{60}} - \rho_{Pb/Si(111)}$) to show the strength of the C$_{60}$-substrate interaction. Without C$_{60}$ adsorbed, the initial wetting layer has the $E_f = -0.70$ eV per Si(111)-(1×1) as also seen in Fig. 2(b). Upon the adsorption of the C$_{60}$ ML, the E_f is enhanced to -0.82 eV per Si(111)-(1×1) by 0.12 eV, which corresponds to an adsorption energy of -0.78 eV per C$_{60}$ on the Pb/Si(111). As shown by $\Delta\rho$ in Fig. 4(a), the interaction is confined to the Pb atoms in the wetting layer as a charge transfer from Pb to C$_{60}$, while Si(111) does not bind directly to C$_{60}$. In contrast, at the other limit ($N_V = 9$) when all the Pb adatoms in the ($\sqrt{7}\times\sqrt{7}$) unit cell are ejected, the C$_{60}$ ML binds strongly on Si(111) forming multiple Si-C covalent bonds at the interface giving an adsorption energy of -5.39 eV per C$_{60}$, or equivalently, -0.77 eV per Si(111)-(1×1). But overall for the whole system, the $E_f(N_V = 0)$ is stronger than $E_f(N_V = 9)$ because of the presence of Pb in the former case.

As Pb is ejected from the unit cell to increase the size of vacancy cluster, E_f first goes less negative quickly and reaches the maximum at $N_V = 3$. The $\Delta\rho$ in Fig. 4(b) shows that although the C$_{60}$-substrate interaction is enhanced, the interaction is still limited to the Pb atoms in the wetting layer and Si(111) atoms still do not bind directly to C$_{60}$. The high energy cost is due to the removal of Pb-Si bonds without compensating C$_{60}$-Si bonds being added. Then as the vacancy cluster size increases to $N_V = 4$, C$_{60}$ starts to bind directly to Si, the stronger interaction shift E_f toward more negative and stabilize the system quickly until it reaches the minimum at $N_V = 7$. The $\Delta\rho$ in Fig. 4(c) at $N_V = 7$ shows the stronger σ-type covalent bonding between Si and C sp orbitals. Finally, as the last two Pb atoms are removed, E_f is reduced again because the newly exposed Si at the interstitial region among C$_{60}$ has no nearby C. The Pb vacancy first appears right underneath C$_{60}$, then expands as a hole when the size of the vacancy cluster increases [see Fig. 4(b) for $N_V = 3$] and reaches the interstitial area among C$_{60}$s [see Fig. 4(c) for $N_V = 7$].

To explain the recent observations on C$_{60}$-induced transformation of the DS phases [12] at such low T, we connect the GS hull across θ and draw the tie line between the two end phases, C$_{60}$/Pb/Si(111) ($N_V = 0$) and C$_{60}$/Si(111) ($N_V = 9$) in Fig. 3. It reveals the thermodynamic stability of C$_{60}$-induced Pb vacancy cluster formation on Pb/Si(111) as a function of N_V. Starting with the full Pb wetting layer sandwiched between the C$_{60}$ ML and Si(111), a single Pb vacancy ($N_V = 1$) has the energy cost of 0.07 eV per Si(111)-(1×1) or 0.46 eV per

C$_{60}$. Vacancy clusters of two and three cost even more energy with the maximum of 0.86 eV (or 0.80 eV in DF1-optPBE) at $N_V = 3$. Vacancy cluster of four is stabilized by starting to form a stronger Si-C$_{60}$ bond, but it is still above the tie line. The stable vacancy clusters are $N_V = 5$, 6, 7, and 8, with $N_V = 7$ being the most stable. The tie line divides the diagram into two regions. The high energy costs of vacancy clusters for $N_V = 1$, 2, 3, and 4 make them inaccessible at the low T $\sim$110 K in experiment [12]. There is a strong thermodynamic driving force to bypass this region and go directly to the stable structures starting with the vacancy clusters $N_V \geqslant 5$.

In the DFT-LDA calculations, the lack of vdW contribution to C$_{60}$-C$_{60}$ interaction has been avoided by taking the C$_{60}$ ML (not an individual C$_{60}$) as the energy reference when calculating E_f in Eq. (1). To evaluate the vdW contribution to C$_{60}$-substrate interaction in the system [38,47], we have used DF1-optPBE to further relax the structures and plot E_f in Fig. 3(b). The vdW interaction enhances the metallic C$_{60}$-Pb bonding (0.8 eV) more than the covalent C$_{60}$-Si bonding (0.4 eV) in terms of C$_{60}$ adsorption energy. But the overall feature in the GS hull and phase stability does not change.

Above we have provided the thermodynamic evidence that the observed transformation of DS phases induced by C$_{60}$ adsorption via Pb atom ejection at low T in the Pb/Si(111) is not by single but multi-atom processes. The DFT calculations give the vacancy cluster of $N_V = 7$ to be the most stable, while the averaged ejection rate from experiment is five Pb atoms per C$_{60}$. This difference can be justified as the following. In experiment [12], the Pb/Si(111) wetting layer was prepared in large uniform ($\sqrt{3}\times\sqrt{7}$) domains with $\theta = 1.20$ ML; a minute density of defects is present which originates from unit cells of the low coverage β-($\sqrt{3}\times\sqrt{3}$) phase with $\theta = 0.33$ ML [see Fig. 2(b)]. Such defects can form during the thermal annealing of the surface at $\sim$480 K to prepare the ($\sqrt{3}\times\sqrt{7}$) phase. Experiment also found that these defect sites are the preferred nucleation sites for C$_{60}$ at the beginning of deposition at low T and thereby the locations to initiate the C$_{60}$-induced reconstruction. C$_{60}$ is highly mobile on the ($\sqrt{3}\times\sqrt{7}$) phase and can reach these well-separated defect sites. This initial C$_{60}$ adsorption at β-($\sqrt{3}\times\sqrt{3}$) defect sites corresponds to the most stable structure found in the DFT, as shown in Fig. 3 with $N_V = 7$ or $\theta = 0.29$ ML. This first group of C$_{60}$ ejects negligible number of Pb atoms because of the small difference in the initial θ and θ after C$_{60}$ adsorption at these defect sites.

With increasing deposition, a second group of C$_{60}$ molecules reach these nucleation sites adsorbing on the adjacent ($\sqrt{3}\times\sqrt{7}$) phase and the ejection process is initiated at these boundaries. The ejected Pb atoms transform very quickly the surrounding area to the next phase in the DS hierarchy. The Pb ejection stops when all the surrounding area has been transformed into the HIC phase. From this point on, with further increase in deposition, the C$_{60}$ island grows in a crystalline structure, i.e., this third group of C$_{60}$ does not contribute further to the ejection rate. So, most C$_{60}$ islands are built from two parts, i.e., a disordered part which ejects Pb adatoms and a crystalline part which does not. There is a height difference between the two parts of approximately 2 Å. The formation of these two parts is consistent with the energetics in Fig. 4 with the disordered part corresponding to
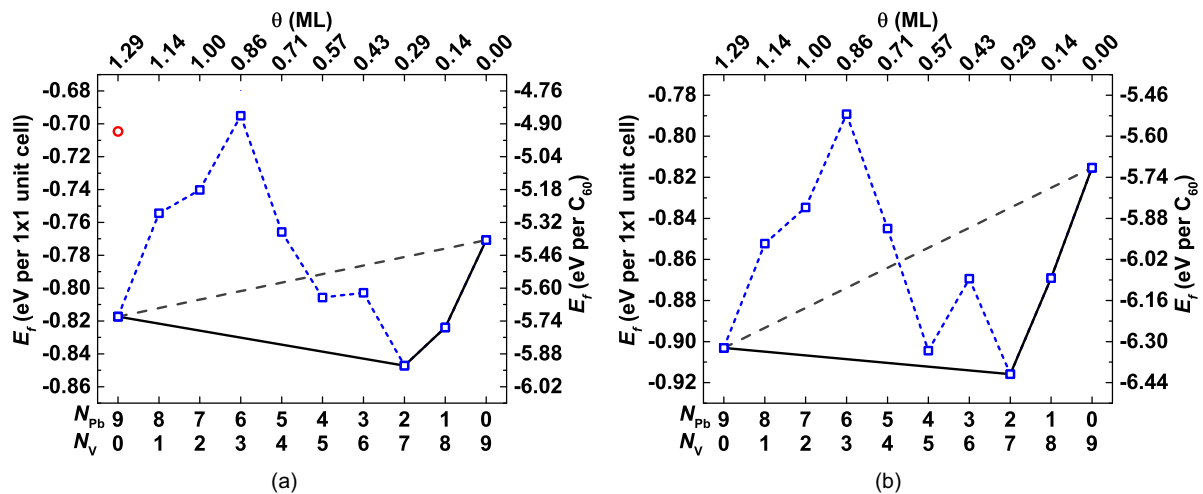
FIG. 3. (Color online) Formation energy (E_f) per Si(111)-(1×1) unit cell (or per C_{60} on the right) in the C_{60}/Pb/Si(111)-($\sqrt{7}\times\sqrt{7}$) surface unit cell calculated with (a) LDA and with (b) DF1-optPBE as a function of the number of vacancies N_V after Pb ejection by the C_{60}. Red circle ($N_V = 0$) corresponds to the initial Pb wetting layer without C_{60}. The phases with $N_V = 0$ and $N_V = 7$ Pb are the most stable with energy minima on opposite side of the most *unstable* phase with $N_V = 3$. The ground state hull is shown by the solid line. The tie (dashed) line between full and zero Pb coverages tells the phase stability vs separating into the two end phases. Including the contribution of the van der Waals interaction in (b) does not affect the relative phase stability.

the energy minimum at $N_V = 7$ [when C_{60}-Si(111) interaction dominates] and the crystalline part corresponding to the energy minimum close to the initial dense layer with no vacancies at $N_V = 0$. An example of how the Pb ejection rate is derived
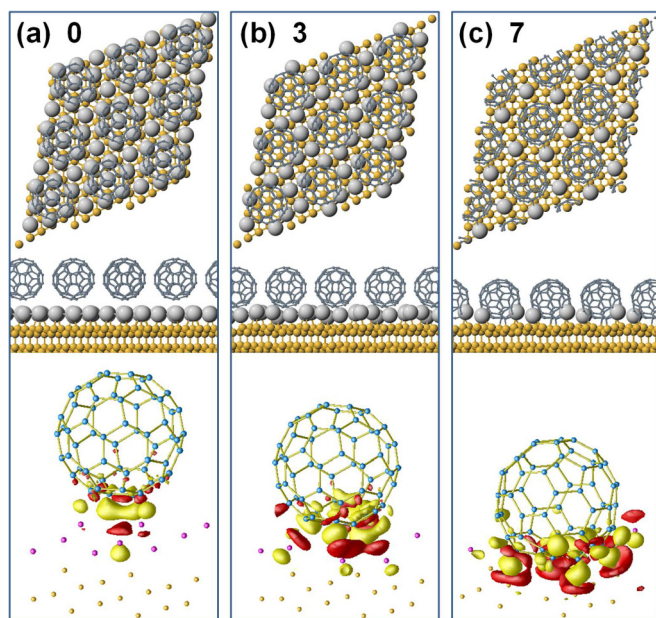

FIG. 4. (Color online) Lowest-energy structures found via thermal annealing in LDA for C_{60}/Pb/Si(111)- ($\sqrt{7}\times\sqrt{7}$) surface unit cell with $N_V = 0$ (a), 3 (b), and 7 (c). The three phases shown are the starting phase and the phases of lowest and highest stability in Fig. 3. The medium brown, large gray, and small gray spheres are for Si, Pb, and C atoms, respectively. In the bottom panel, red (yellow) iso-surfaces are shown for electron depletion (accumulation), $\Delta\rho = \rho_{C_{60}/Pb/Si(111)} - \rho_{C_{60}} - \rho_{Pb/Si(111)}$, at $\pm 0.7 \times 10^{-2}$ e/Å^3 (a), $\pm 1.4 \times 10^{-2}$ e/Å^3 (b), and $\pm 2.7 \times 10^{-2}$ e/Å^3 (c). The brown, magenta, and blue spheres are for Si, Pb, and C atoms, respectively.

in the experiment is shown in Fig. 4 of Ref. [12]. An area transforms to the DS(2,1) phase from the initial ($\sqrt{3}\times\sqrt{7}$) phase with 56 Pb atoms added and the adjacent C_{60} island contains 11 randomly nucleated C_{60}. The ejection rate of ~5 per C_{60} is averaged over both the first group of C_{60} adsorbing on β-($\sqrt{3}\times\sqrt{3}$) with no Pb ejection and the second group of C_{60} (before crystallization).

IV. DISCUSSION

The C_{60}/Pb/Si(111) experiment was used to deduce intriguing results about the diffusion mechanism from the comparison of the final and initial state of the DS transformation, but not all the in-between steps because the STM is not a real time technique due to its slow acquisition speed. As noted in Ref. [12], no diffusing Pb adatoms are ever seen on top of the wetting layer after the ejection, the DS rows are practically completed (within the shortest time approximately tens of seconds to collect the STM image or to record the LEED pattern) and the DS rows mysteriously develop only on one side of the C_{60} island (which is not possible if the transformation to the next DS phase was due to single Pb adatom diffusion in classical random walk). Because each DS phase involves a complex pattern and the arrival and attachment of the ejected Pb atoms should be in exact locations for this new pattern to be built error-free (as seen in the experiment), this perfect transformation was found to be unusually fast. It leads to a negative activation energy for the diffusion coefficient—if it is assumed to be random walk diffusion of single Pb adatoms; therefore it implies that mass transport must be through the collective motion of the wetting layer—consistent with other unusual observations about Pb/Si(111) found in concentration profile evolution with LEEM [9,10], Pb(111) island nucleation experiments with STM, and coarsening experiments at higher coverage from x-ray diffraction [11]. Our current DFT study supplies the missing evidence on

the type of atomistic processes for the unusual collective mechanism needed to account for the speed of the phase transformation in Pb/Si(111). There is a highly unstable size range for vacancy clusters with an energy barrier $\sim$0.8 eV, between the two minima in Fig. 3, the phases with $N_V = 0$ and 7. It cannot be overcome at 110 K by ejected Pb atoms if they are removed successively, so collective multi-atom processes must be involved.

V. SUMMARY

We have studied the structural energetics of C$_{60}$-induced Pb ejection in the C$_{60}$/Pb/Si(111) system to provide the evidence for multi-atom processes need for the superfast DS transformation observed in experiment. By introducing the Pb/Si(111)-($\sqrt{7}\times\sqrt{7}$) unit cell [which is as stable as the initial ($\sqrt{3}\times\sqrt{7}$) and the DS phases], but with the advantage to accommodate a hexagonal C$_{60}$ monolayer, we have calculated the vacancy formation energy in C$_{60}$/Pb/Si(111) system as a function of Pb vacancy cluster size (or equivalently the number of ejected Pb atoms). From the formation energy diagram, it is clearly seen that small vacancy clusters of

1–4 have high energy cost and are not thermodynamically favored. Stable vacancy clusters are possible for sizes larger than five (with seven being the most stable), in good agreement with the estimated ejection rate of five Pb atoms per C$_{60}$ in the experiment, which is an average over all the C$_{60}$ that have joined the island. The large energy barrier $\sim$0.8 eV (Fig. 3) separating the high and low Pb-coverage stable phases excludes random walk diffusion as being the mechanism for mass transport. This confirms that multi-atom processes must be responsible for the unusually fast and correlated diffusion transforming an initial DS to the phase next in the hierarchy, a type of transport process rarely seen in nature.

[1] R. Plass, J. A. Last, N. C. Bartelt, and G. L. Kellogg, Nanostructures—Self-assembled domain patterns, Nature (London) **412**, 875 (2001).

[2] Y. Sato, S. Chiang, and N. C. Bartelt, Spontaneous Domain Switching During Phase Separation of Pb on Ge(111), Phys. Rev. Lett. **99**, 096103 (2007).

[3] J. de la Figuera, F. Leonard, N. C. Bartelt, R. Stumpf, and K. F. McCarty, Nanoscale Periodicity in Stripe-Forming Systems at High Temperature: Au/W(110), Phys. Rev. Lett. **100**, 186102 (2008).

[4] T. O. Mentes, A. Locatelli, L. Aballe, and E. Bauer, Stress Induced Stripe Formation in Pd/W(110), Phys. Rev. Lett. **101**, 085701 (2008).

[5] N. H. P. Nguyen, D. Klotsa, M. Engel, and S. C. Glotzer, Emergent Collective Phenomena in a Mixture of Hard Shapes through Active Rotation, Phys. Rev. Lett. **112**, 075701 (2014).

[6] H. J. Zhao, V. R. Misko, and F. M. Peeters, Analysis of pattern formation in systems with competing range interactions, New J. Phys. **14**, 063032 (2012).

[7] M. Hupalo and M. C. Tringides, Ultrafast kinetics in Pb/Si(111) from the collective spreading of the wetting layer, Phys. Rev. B **75**, 235443 (2007).

[8] M. Yakes, M. Hupalo, M. A. Zaluska-Kotur, Z. W. Gortel, and M. C. Tringides, Low-Temperature Ultrafast Mobility in Systems with Long-Range Repulsive Interactions: Pb/Si(111), Phys. Rev. Lett. **98**, 135504 (2007).

[9] K. L. Man, M. C. Tringides, M. M. T. Loy, and M. S. Altman, Anomalous Mass Transport in the Pb Wetting Layer on the Si(111) Surface, Phys. Rev. Lett. **101**, 226102 (2008).

[10] K. L. Man, M. C. Tringides, M. M. T. Loy, and M. S. Altman, Superdiffusive Motion of the Pb Wetting Layer on the Si(111) Surface, Phys. Rev. Lett. **110**, 036104 (2013).

[11] M. T. Hershberger, M. Hupalo, P. A. Thiel, C. Z. Wang, K. M. Ho, and M. C. Tringides, Nonclassical "Explosive" Nucleation in Pb/Si(111) at Low Temperatures, Phys. Rev. Lett. **113**, 236101 (2014).

[12] A. V. Matetskiy, L. V. Bondarenko, D. V. Gruznev, A. V. Zotov, A. A. Saranin, and M. C. Tringides, Structural transformations in Pb/Si(111) phases induced by C-60 adsorption, J. Phys.-Condens. Matter **25**, 395006 (2013).

[13] M. Hupalo, J. Schmalian, and M. C. Tringides, "Devil's staircase" in Pb/Si(111) Ordered Phases, Phys. Rev. Lett. **90**, 216106 (2003).

[14] P. Bak and R. Bruinsma, One-Dimensional Ising-Model and the Complete Devils Staircase, Phys. Rev. Lett. **49**, 249 (1982).

[15] E. Granato, S. C. Ying, K. R. Elder, and T. Ala-Nissila, Anomalous Fast Dynamics of Adsorbate Overlayers Near an Incommensurate Structural Transition, Phys. Rev. Lett. **111**, 126102 (2013).

[16] L. Huang, C. Z. Wang, M. Z. Li, and K. M. Ho, Coverage-Dependent Collective Diffusion of a Dense Pb Wetting Layer on Si(111), Phys. Rev. Lett. **108**, 026101 (2012).

[17] A. J. Maxwell, P. A. Bruhwiler, D. Arvanitis, J. Hasselstrom, M. K. J. Johansson, and N. Martensson, Electronic and geometric structure of C$_{60}$ on Al(111) and Al(110), Phys. Rev. B **57**, 7312 (1998).

[18] M. Stengel, A. De Vita, and A. Baldereschi, Adatom-Vacancy Mechanisms for C$_{60}$/Al(111)-(6×6) Reconstruction, Phys. Rev. Lett. **91**, 166101 (2003).

[19] R. Felici, M. Pedio, F. Borgatti, S. Iannotta, M. Capozi, G. Ciullo, and A. Stierle, X-ray-diffraction characterization of Pt(111) surface nanopatterning induced by C$_{60}$ adsorption, Nat. Mater. **4**, 688 (2005).

[20] X. Q. Shi, A. B. Pang, K. L. Man, R. Q. Zhang, C. Minot, M. S. Altman, and M. A. Van Hove, C$_{60}$ on the Pt(111) surface: Structural tuning of electronic properties, Phys. Rev. B **84**, 235406 (2011).

[21] H. I. Li, K. Pussi, K. J. Hanna, L. L. Wang, D. D. Johnson, H. P. Cheng, H. Shin, S. Curtarolo, W. Moritz, J. A. Smerdon, R. McGrath, and R. D. Diehl, Surface Geometry of C_{60} on Ag(111), Phys. Rev. Lett. **103**, 056101(2009).

[22] K. Pussi, H. I. Li, H. Shin, L. N. S. Loli, A. K. Shukla, J. Ledieu, V. Fournee, L. L. Wang, S. Y. Su, K. E. Marino, M. V. Snyder, and R. D. Diehl, Elucidating the dynamical equilibrium of C_{60} molecules on Ag(111), Phys. Rev. B **86**, 205406 (2012).

[23] G. Schull, N. Neel, M. Becker, J. Kroger, and R. Berndt, Spatially resolved conductance of oriented C(60), New J. Phys. **10**, 065012 (2008).

[24] X. Torrelles, M. Pedio, C. Cepek, and R. Felici, $(2\sqrt{3}\times 2\sqrt{3})R30°$ induced self-assembly ordering by C_{60} on a Au(111) surface: X-ray diffraction structure analysis, Phys. Rev. B **86**, 075461 (2012).

[25] H. Shin, A. Schwarze, R. D. Diehl, K. Pussi, A. Colombier, E. Gaudry, J. Ledieu, G. M. McGuirk, L. N. S. Loli, V. Fournee, L. L. Wang, G. Schull, and R. Berndt, Structure and dynamics of C_{60} molecules on Au(111), Phys. Rev. B **89**, 245428 (2014).

[26] W. W. Pai, H. T. Jeng, C. M. Cheng, C. H. Lin, X. D. Xiao, A. D. Zhao, X. Q. Zhang, G. Xu, X. Q. Shi, M. A. Van Hove, C. S. Hsue, and K. D. Tsuei, Optimal Electron Doping of a C_{60} Monolayer on Cu(111) via Interface Reconstruction, Phys. Rev. Lett. **104**, 036103 (2010).

[27] G. Xu, X. Q. Shi, R. Q. Zhang, W. W. Pai, H. T. Jeng, and M. A. Van Hove, Detailed low-energy electron diffraction analysis of the (4×4) surface structure of C_{60} on Cu(111): Seven-atom-vacancy reconstruction, Phys. Rev. B **86**, 075419 (2012).

[28] P. Hohenberg and W. Kohn, Inhomogeneous electron gas, Phys. Rev. **136**, B864 (1964).

[29] W. Kohn and L. J. Sham, Self-consistent equations including exchange and correlation effects, Phys. Rev. **140**, A1133 (1965).

[30] S. Stepanovsky, M. Yakes, V. Yeh, M. Hupalo, and M. C. Tringides, The dense α-$\sqrt{3}$x$\sqrt{3}$Pb/Si(111) phase: A comprehensive STM and SPA-LEED study of ordering, phase transitions and interactions, Surf. Sci. **600**, 1417 (2006).

[31] X. H. Lu, M. Grobis, K. H. Khoo, S. G. Louie, and M. F. Crommie, Spatially Mapping the Spectral Density of a Single C_{60} Molecule, Phys. Rev. Lett. **90**, 096802 (2003).

[32] L. L. Wang and H. P. Cheng, Rotation, translation, charge transfer, and electronic structure of C_{60} on Cu(111) surface, Phys. Rev. B **69**, 045404 (2004).

[33] L. L. Wang and H. P. Cheng, Density functional study of the adsorption of a C_{60} monolayer on Ag(111) and Au(111) surfaces, Phys. Rev. B **69**, 165417 (2004).

[34] X. H. Lu, M. Grobis, K. H. Khoo, S. G. Louie, and M. F. Crommie, Charge transfer and screening in individual C_{60}

molecules on metal substrates: A scanning tunneling spectroscopy and theoretical study, Phys. Rev. B **70**, 115418 (2004).

[35] M. Feng, J. Zhao, and H. Petek, Atomlike, hollow-core-bound molecular orbitals of C_{60}, Science **320**, 359 (2008).

[36] G. Schull, T. Frederiksen, M. Brandbyge, and R. Berndt, Passing Current Through Touching Molecules, Phys. Rev. Lett. **103**, 206803 (2009).

[37] L. Tang, X. Zhang, Q. M. Guo, Y. N. Wu, L. L. Wang, and H. P. Cheng, Two bonding configurations for individually adsorbed C_{60} molecules on Au(111), Phys. Rev. B **82**, 125414 (2010).

[38] I. Hamada and M. Tsukada, Adsorption of C_{60} on Au(111) revisited: A van der Waals density functional study, Phys. Rev. B **83**, 245437 (2011).

[39] X. Q. Shi, M. A. Van Hove, and R. Q. Zhang, Adsorbate-induced reconstruction by C_{60} on close-packed metal surfaces: Mechanism for different types of reconstruction, Phys. Rev. B **85**, 075421 (2012).

[40] J. P. Perdew and A. Zunger, Self-interaction correction to density-functional approximations for many-electron systems, Phys. Rev. B **23**, 5048 (1981).

[41] D. M. Ceperley and B. J. Alder, Ground State of the Electron Gas by a Stochastic Method, Phys. Rev. Lett. **45**, 566 (1980).

[42] M. Dion, H. Rydberg, E. Schroder, D. C. Langreth, and B. I. Lundqvist, van der Waals Density Functional for General Geometries, Phys. Rev. Lett. **92**, 246401 (2004).

[43] J. Klimes, D. R. Bowler, and A. Michaelides, van der Waals density functionals applied to solids, Phys. Rev. B **83**, 195131 (2011).

[44] P. E. Blöchl, Projector augmented-wave method, Phys. Rev. B **50**, 17953 (1994).

[45] G. Kresse and J. Furthmüller, Efficient iterative schemes for *ab initio* total-energy calculations using a plane-wave basis set, Phys. Rev. B **54**, 11169 (1996).

[46] G. Kresse and J. Furthmüller, Efficiency of *ab-initio* total energy calculations for metals and semiconductors using a plane-wave basis set, Comput. Mater. Sci. **6**, 15 (1996).

[47] K. Berland and P. Hyldgaard, Analysis of van der Waals density functional components: Binding and corrugation of benzene and C_{60} on boron nitride and graphene, Phys. Rev. B **87**, 205421 (2013).

[48] L. L. Wang and D. D. Johnson, Density functional study of structural trends for late-transition-metal 13-atom clusters, Phys. Rev. B **75**, 235405 (2007).

[49] T. L. Chan, C. Z. Wang, M. Hupalo, M. C. Tringides, Z. Y. Lu, and K. M. Ho, First-principles studies of structures and stabilities of Pb/Si(111), Phys. Rev. B **68**, 045410 (2003).